Elsevier Editorial System(tm) for Nuclear Inst. and Methods in Physics Research, A
Manuscript Draft

Manuscript Number:

Title: Extended-time-scale creep measurement on Maraging cantilever blade springs.

Article Type: Research Paper

Section/Category: Special Applications

Keywords: maraging; creep; Young's modulus thermal variation; Arrhenius acceleration; seismic isolation

Corresponding Author: Miss Nicole Virdone,

Corresponding Author's Institution: California Institute of Technology

First Author: Nicole Virdone

Order of Authors: Nicole Virdone; Juri Agresti; Alessandro Bertolini; Riccardo DeSalvo; Rosalia Stellacci; Justin Kamp; Maddalena Mantovani; Virginio Sannibale; Marco Tarallo; Lisa Kaltenegger

Manuscript Region of Origin:

Abstract: Two controlled temperature facilities were built to induce an accelerated creep rate in a Maraging steel GAS spring and to measure the material's creep over an artificially extended period of time. The data acquisition of the first experiment lasted for almost a year, but then the blades were allowed to creep for six more years before measuring the permanent deformation integrated over time. The data from this first experiment was polluted by a defect in the data acquisition software, but yielded overall creep limits and an evaluation of the Arrhenius acceleration of creep speed with temperature (1.28±0.13/oC). The duration of the second experiment was only one year but more free of systematic errors. The effective test period of this second experiment (normalized with the Arrhenius acceleration measured in the first experiment) extends in the billions of years showing no sign of anomalous creep. The result of both experiments also produced a simple procedure capable of eliminating all practical effects of creep from the Advanced LIGO seismic isolation and suspensions. Measurements of creep under various stress levels, and of the thermal variations of Young's modulus (2.023 (±0.013) 10-4/oC) are reported as well.

Extended-time-scale creep measurement on Maraging cantilever blade springs.

Nicole Virdone[1,2], Juri Agresti[2,3], Alessandro Bertolini [7], Riccardo DeSalvo[2], Rosalia Stellacci [2,3,5], Justin Kamp [6], Maddalena Mantovani[2,3,4], Virginio Sannibale[2], Marco Tarallo[2,3], Lisa Kaltenegger [8]

1 Mayfield Senior High School, 500 Bellefontaine St, Pasadena, CA 91105-USA, now at University of California - Los Angeles, 405 Hilgard Ave, Los Angeles, CA 90095-USA

2 LIGO Observatories, California Institute of Technology, Pasadena, CA 91125-USA

3 Dipartimento di Fisica "Enrico Fermi" and INFN Sezione di Pisa, Università di Pisa, Largo Bruno Pontecorvo, I-56127 Pisa, Italy

4 now at Università di Siena, dipartimento di Fisica - Via Roma, 56, I-53100Siena, Italy

5 now at Università degli Studi di Napoli Federico II - Corso Umberto I, I-80138 Napoli, Italy

6 now at Chalmers University of Technology, SE-412 96 Goteborg, Sweden

7 now at DESY, Forschung Linear Collider Division, Notkestrasse 85, D-22607 Hamburg, Germany

8 now at Harvard Smithsonian Institute for Astrophysics (CfA), 60 Garden Street, Cambridge, MA 02138

Send Proofs to:

Nicole Virdone

Postal Address: 415 Gayley Ave. Apt. 105; Los Angeles, CA 90024
Phone: (626) 379-0873
Email: nvirdone@ucla.edu; nvirdone@gmail.com

Abstract

Two controlled temperature facilities were built to induce an accelerated creep rate in a Maraging steel GAS spring and to measure the material's creep over an artificially extended period of time. The data acquisition of the first experiment lasted for almost a year, but then the blades were allowed to creep for six more years before measuring the permanent deformation integrated over time. The data from this first experiment was polluted by a defect in the data acquisition software, but yielded overall creep limits and an evaluation of the Arrhenius acceleration of creep speed with temperature ($1.28\pm0.13/^{o}C$). The duration of the second experiment was only one year but more free of systematic errors. The effective test period of this second experiment (normalized with the Arrhenius acceleration measured in the first experiment) extends in the billions of years showing no sign of anomalous creep. The result of both experiments also produced a simple procedure capable of eliminating all practical effects of creep from the Advanced LIGO seismic isolation and suspensions. Measurements of creep under various stress levels, and of the thermal variations of Young's modulus ($2.023\ (\pm0.013)\ 10^{-4}/^{o}C$) are reported as well.

Classification codes:

62.20.Hg Creep
61.72.Hh Indirect evidence of dislocations and other defects (resistivity, slip, creep, strains, internal friction, EPR, NMR, etc.)
62.20.de Elastic moduli
62.20.fq Plasticity and superplasticity

Key Words:
Maraging; creep; Young's modulus thermal variation; Arrhenius acceleration; seismic isolation

Footnotes

Conversely, if creep was to completely relax the radial compression without changing the energy stored in the bending that is holding up the load, only the resonant frequency would be changed and not the vertical equilibrium position.

[2] The linear droop of an unconstrained blade can be obtained by rescaling the measured droop with the square of ratio of the resonant frequencies times a small correction factor of the order of one. Considering that we have observed that changing the radial compression does not change the vertical equilibrium point, one can estimate this correction factor to be very close to unity.

[3] Of course any real-life creep relieving procedure would be designed to maintain the metal well below the plastic transition and thus avoid any danger of plastic slippage.

1. Introduction

All material under stress experiences a measurable creep, which is an increase of its strain over time. Creep is normally a very slow process involving movement of dislocations inside the material's grains. Its effect on springs supporting a load is to reduce the "lifting" power of the spring over time and allow its payload to droop. The main source of creep is the dislocations' movement, which is normally impeded by the anchoring of dislocations to other discontinuities of the crystalline matrix. Some dislocations get freed by local fluctuations of thermal energy, drift down the stress field until they encounter the next obstacle, and thus generate creep. Dislocation activation is therefore most likely to occur at higher temperatures following the Arrhenius law. In the absence of dislocation regeneration, creep is generated using up the available dislocations. As a consequence, the creep behavior at a constant temperature is expected to be logarithmic with time, while if the temperature rises, the creep simply accelerates according to the Arrhenius law [1].

If the temperature is increased excessively, new dislocations may appear or become activated and the creep behavior changes, normally switching from logarithmic to linear.

All Gravitational Wave interferometers use or propose to use chains of cantilever blade springs to support the mirror test masses and isolate them from seismic noise. All, to some level, are affected by creep problems. In Ad-LIGO, blade-springs are made with a metal alloy called Maraging steel, which has particularly good creep characteristics [2].

We made two experiments to characterize the creep in Maraging steel. In both cases we used temperature to accelerate the creep speed. The first experiment was performed with unconstrained cantilever blades, each loaded with a free hanging ballast mass and read-out with a LVDT position transducer. The blades were attached to the sides of a column, housed in a large oven with a thermal stabilization of 10 m^{o}K/week.

In the second test we took advantage of the Geometric Anti Spring (GAS) configuration to cancel the restoring forces and thus enhance the effects of creep.

The GAS filters, initially developed for use in Advanced LIGO [3,7,8], are one of the most efficient vertical seismic noise attenuation systems. Conceptually similar to VIRGO's magnetic anti-spring filters [9], they use a symmetric arrangement of strong, contrapposed, triangular cantilever blades to form a system where the spring restoring forces can be reduced or even cancelled at will (Please refer to [22] for a simple explanation and schematic view of a GAS filters).

The cantilever blades of a GAS filter are originally flat and bend under load. They are linked to a central keystone, or load disk, and are subject to radial compression. All radial forces cancel out by symmetry. The dimensioning of the blades is chosen to support the desired payload at the point of maximal radial compression.

Any deviation from that working point results in a reduction of compressional energy, in its turn resulting in a force proportional to the displacement, just as in a normal spring, but with the opposite sign (anti-spring).

Tuning the blades' radial compression changes the anti-spring strength. This can be done to null the vertical stiffness of the blades, giving the GAS system its "soft spring" qualities without changing the vertical force supporting the payload. The blade's profile

is chosen so that a constant stress is imposed anywhere along the blades. The filter can be sized to lift any payload, imposing any arbitrary stress in the material, and obtaining any vertical spring stiffness (vertical resonant frequency) all at the same time.

The GAS configuration, which is designed to reduce the resonant frequency of vertical oscillators, is ideal to study creep properties of materials because of its tunable stiffness and uniform stress in the material. The restoring force cancellation of the GAS mechanism results in tunable sensitivity to the creep effects (and with the same amplification factor, to the effects of hysteresis and thermal variations of the Young's modulus), while the full spring lift capabilities are maintained. The visibility of these effects is enhanced by the square of the resonant frequency reduction factor [11]. The GAS springs are particularly well suited for this kind of test because they have, by design, uniform stress throughout the entire blade surfaces (the profile of the blades is carefully calculated to produce constant radius of curvature (stress) along the entire blade length [12]) without increasing the overall stress applied on the spring material.

In a vertical oscillator made of normal (unconstrained) springs the energy is periodically exchanged between gravitational and elastic potential energy at the two end points of the excursion, via the kinetic energy.

In the GAS spring oscillator, a fraction of what would be kinetic energy is stored in a mechanical potential energy reservoir (the variation of radial compression) largely independent from the one storing the energy of the vertical movement. This reservoir stores a very small fraction (few percent) of the overall elastic potential energy. Since the lift is obtained by integration along the blade length of the stress relative to the vertical

bending (the radial compression does not contribute to the lift), only the creep of the stress of the material contributing to the vertical force can be expected to count in lowering the payload[1]. Since the vertical component of the stress is the same as in an unconstrained blade, the GAS principle cannot be expected to significantly change the amount of energy lost in creep and, while the droop is greatly amplified, the creep-induced loss of lifting power, measured in Newton, is substantially the same as would be in an unconstrained cantilever spring under the same load and stress[2]. Therefore the measurements reported in this paper remain valid for any spring configuration made with similarly hardened Maraging steel.

To make a representative test, creep was measured with a geometry (and stress level) identical to the spring used in the SAS systems in TAMA (680 MPa) and in the seismic attenuation system developed for Advanced LIGO [reference Alberto Stochino doctoral thesis]. This stress level is also similar to the stress level used in the LIGO multiple pendulums, i.e. of the order 800 to 1000 MPa. The thickness of the blade is 2.25mm and the radius of curvature is 240mm. The peak strain level in the blades of the filter we tested is 0.0047.

Since creep is generated by thermal fluctuations, it occurs in a shorter time frame at higher temperatures following an Arrhenius exponential law. The ensuing raise in the

[1] Conversely, if creep was to completely relax the radial compression without changing the energy stored in the bending that is holding up the load, only the resonant frequency would be changed and not the vertical equilibrium position.

[2] The linear droop of an unconstrained blade can be obtained by rescaling the measured droop with the square of ratio of the resonant frequencies times a small correction factor of the order of one. Considering that we have observed that changing the radial compression does not change the vertical equilibrium point, one can estimate this correction factor to be very close to unity.

creep rate at higher temperatures is equivalent to an acceleration of time. To calculate the time acceleration, we conservatively assumed an Arrhenius thermal acceleration of the creep rate of ~1.175 /^{o}C (which is close to the lower limit of our acceleration measurements). The estimation of this acceleration is discussed in Section 5. Although this number is not very well measured, its actual value is only marginally important for the development of a procedure to eliminate, to all practical purposes, the ill effects of creep. Baking the structure under its nominal stress at moderate temperatures allows for an effective ageing equivalent to very long time periods. With the assumed time acceleration value, and a heating at only 150^{o}C, we calculated that the creep speed increases by a factor of at least 8.8 x 10^{8}. Thus at 150°C, the creep measured in a day corresponds to what it would experience in 2.4 million years.

The most important result is the accelerated burnout of the dislocations that would have moved over the expanded time frame, and thus a drastic reduction of any further droop after the specified heat process.

Of course if the temperature were raised beyond a certain threshold, other effects inducing plasticity (new dislocations) would start.

The onset of any of these processes would be signaled by a marked increase of creep and the appearance of a constant creep speed (or even growing with time). Cobalt, Nickel and Titanium precipitates, interspersed within the martensitic structure of the material grains, pin down the dislocations in Maraging. When exceeding the elasticity limit, the dislocations are expected to simply jump over the precipitates that pinned them. As these precipitates are all statistically equal, the transition is expected to be sharp. After

exceeding the elasticity limit, Maraging is expected to transition to a completely plastic material [13].

The sharp beginning of such a runaway creep was observed, at our stress levels, between 190 and 200^{o}C, detected by monitoring the creep speed while increasing the temperature. Having identified the stress and temperature levels that induce runaway creep, controlled baking procedures of the blades under nominal stress can be designed to eliminate all practical effects of creep.

For any Arrhenius creep acceleration rate within the limits measured in Section 5, the exponential increase of creep speed ensures that, to all practical purposes, all available dislocations can be burned out and creep stopped, with bake out periods of the order of a few days at temperatures only ~100^{o}C above room temperatures and without changing the spring's characteristics.

These bakeout conditions are similar and compatible to that recommended for standard Ultra-High Vacuum bakeout procedures.

2. Materials and Method

We built two creep measurement setups. The first one, built in the year 2000, is described in Section 4. The second was built in 2004 and is described below.

An oven withstanding temperatures up to 200° C was built to house a 60 cm diameter TAMA-SAS GAS filter [14].

A 5-10 mm thick aluminum inner lining of the oven ensured good thermal uniformity. An air gap of at least 1cm thickness was allowed all around between the filter and the oven

inner lining. A heating tape wrapped around the oven's inner lining and controlled by a PID temperature controller was used to stabilize the oven temperature at the desired temperature within a fraction of a degree Celsius. The feedback thermocouple was suspended in air, inside the oven volume. Control thermometers were hooked directly on the surface of a blade and outside of the oven. The GAS filter, consisting of a three-blade unit, was tuned to 0.86 Hz (effective elastic constant K = 2200 N/m, a very moderate GAS tuning). The stainless steel filter frame, with virtually the same thermal expansion coefficient of the Maraging blades, practically eliminated all differential thermal expansion effects. A small hole at the bottom of the oven allowed the passage of the wire supporting the external 63.7±0.2 kg payload. Care was taken so that the wire had a clearance of about 1 mm in all directions. A 5 cm thick, semi-rigid high-thermal-insulation foam jacket, precision cut and held by an external steel lining, allowed for no air circulation between the inside and the outside of the oven. The filter body was supported through rigid, thin-wall stainless steel pipe spacers running between the filter body and the inner lining, as well as across the thermal insulation jacket.

An external mechanical gauge was connected to the wire to measure the relative height of the payload with respect to the support of the filter body [17]. Proper care was taken to ensure that the gauge was not exposed, or in any way affected by the internal temperature of the oven. The droop of the payload can be easily measured with this gauge to a precision of 10 microns. We used a mechanical gauge because of its simplicity, while providing an absolute measurement of the payload droop. The main disadvantage of a mechanical gauge was the noise introduced by its sticks and slip friction, which is significant against the softness of the filter.

Measurements were performed by manually exciting the vertical oscillation of the spring and recording the end position read by the gauge. If multiple measurements are graphed in a histogram, the stick and slip of the mechanical gear in the gauge produce a characteristic double peak distribution (Figure 1) corresponding to whichever direction, up or down, the movement stopped. This noise can be mitigated by performing many measurements (typically 60) at a specific time, thus averaging out the systematic error introduced by the stick and slip bi-stability to acceptable levels (10-20 ⌈m). This procedure also eliminates all material hysteresis effects encountered in static measurements (see discussion of data of figure 11 in section 5).

Figure 1: Typical double horn structure of a vertical position measurement.

To characterize the temperature behavior of the system, the oven was first heated to 30°C, then up to 40°C, and finally back down to 30°C. During this initial series, the vertical height of the payload was measured many times per day for a week at both temperature levels. In Section 6, our measurements showed that the Young modulus of the blades decreases by ~2 x $10^{-4}/^{o}$C. This large effect is rapid (several hours of thermalization; also see the discussion of Figure 10 in Section 6) as compared with the observed creep times (~days) and fully reversible. Due to its reversibility, it can be subtracted from the creep effect by simply returning to an original, lower temperature level after each period at higher temperature. Unfortunately this effect also masks the instantaneous change of creep slope induced by temperature variations that would otherwise allow precise measurement of the Arrhenius rate of creep acceleration. The

measurements of thermal variation of the Arrhenius creep rate acceleration and of the Young's modulus are detailed in Sections 5 and 6 respectively.

After the starting measurements between 30 and 40°C, we adopted a baseline temperature of 40°C for the rest of the experiment. We chose this temperature because it is sufficiently above room temperature and allows for rapid returns and for stable oven temperature controls. We then took measurements at monotonically increasing temperature levels, each followed by a return to the 40°C baseline level. At each temperature level, daily creep measurements were taken over (typically) two-week periods, followed by a week of measurements at the baseline temperature of 40°C. Each daily measurement consisted of about 60 individual position measurements averaged to mitigate the stick and slip measurement error. The temperature levels we examined are listed in Table 1.

At the end we performed a final, long measurement, at the 40°C baseline temperature. In the final run, the measurements were taken only twice a week but for a much longer period of time (118 days) to verify the elimination of creep (within the measurement sensitivity) expected from our process.

It should be noted that every time we increased the temperature, the GAS blades rapidly relaxed due to the ~2. 10^{-04} x 10^{-4}/°C change of Young's modulus. In order to maintain the GAS filter near its working point, and at as closely as possible a constant strain level, in the measurements above 90°C we removed some weight from the payload, and carefully replaced it when returning to the baseline 40°C. This procedure maintained, to all practical purposes, a constant strain level on the blades and did not affect the measurement of the absolute value of the creep within each temperature cycle.

3. Creep Measurement Results

The initial creep at each temperature level is mostly masked by the movements generated by the thermal Young's modulus variations. Thermalization is limited to the first hours after each temperature change. The manual readout of this setup is not well suited to follow it and, after the kickoff measurements illustrated in Figure 2, we did not even try to track it. Each measurement at high temperature shows the initial drop due to the change of Young's modulus, followed by the logarithmic droop. A measurement (excluding the initial transient) is shown in Figure 3. The aim of these measurements is to verify that a creep saturation level is reached (the logarithmic creep dropped below the measurement sensitivity), and that no macroscopic slope (plasticity) is appearing. The duration of each step at a specific temperature is also carefully recorded. The measurement back to the 40^{o}C baseline (Figure 2) is used to measure the creep integrated over the preceding "at temperature" period while eliminating the effects of the thermal changes of Young's modulus.

Figure 2: Typical transient at a temperature change (returning to 40^{o}C). The undershoot is attributed to thermal variations of the Young's module induced by oven temperature fluctuation before the PID controller stabilizes the temperature, and to differential heating of the parts. The oven response is slower in descending temperature steps.

Figure 3: Creep behavior observed at 90°C. The initial creep, masked by the droop caused by the thermal variations of Young's modulus, is missed in this measurement.

Occasionally unexplained steps were observed (Figure 4). If they were stress related, the slippage would only be downward. As we observed steps in both directions we attributed them to some bistability of our support setup. These unphysical steps are the largest limiting factor of these measurements.

Figure 4: Two unexpected large readout position jumps, ~100 mm downwards observed on day 12 at 40°C (left graph) and ~ 70 mm upwards observed on day 27 at 60°C. These jumps were attributed to some external structure bi-stability. The observed jumps are significantly smaller than the observed creep, and represent our largest experimental uncertainty.

For most of the observed temperature levels, the data closely followed the logarithmic decay. A progressive droop, adding up to a total of about 1.5 mm from the beginning of the experiment (Table 1 cycle 13, and Figure 5), was measured returning from the second highest cycle at 190°C back to 40° C. Considering the effective blade bending $l = \frac{g}{\omega^2} = 336mm$ of the GAS filter used, this drop corresponds to a 0.44% increase of the initial blade bending or an equivalent 0.44% loss of lifting power at constant position. In other words, the measured fractional loss of lifting power at constant position is proportional to the load, but not proportional to the frequency of the filter. A 0.44% increase of the initial blade bending can be expected from any Maraging cantilever blade

subject to the same stress level, with most of the effect showing up within the first year of service. As previously discussed, baking the filter under load corresponds to leaving the spring under load for an extended period of time. If we consider the exponential stretch of time induced by higher temperatures, and that the creep is expected to be a logarithm of time, the data can be best summarized in the log-time plot of Figure 5. The linear fit in Figure 5 is in excellent agreement, over many orders of magnitude, with the expected logarithmic character of creep. With the assumed time expansion of a factor of 5 every 10°C, the integrated effective experiment duration is equivalent to suspending the payload for 10^{12} years (the time scale would be almost a million times longer if we had used the most probable creep acceleration factor of Table 1).

Table 1: Measured creep data. The time expansion factor is obtained using creep acceleration rate of 1.174/^{o}C (corresponding to an assumed factor of 5 per 10^{o}C temperature increase). The effective ageing time (column 7) is obtained multiplying column 4 by column 6.

Figure 5: Integrated creep as a function of integrated effective ageing time. Only the measurements up to 190^{o}C of table 1 are used in this plot because of the different observed creep at 200^{o}C. The dot size corresponds to a measurement error of 30 microns.

Figure 6: Linear creep rate observed when raising the oven temperature to 200^{o}C. The fit is compatible with a linear slope of 18+/-1 mm/day.

The oven maximum temperature was 200°C. When the temperature was raised from 190°C to 200°C an onset of linear creep behavior was detected (Figure 6) in sharp contrast with the logarithmic behavior seen at lower temperatures. This very sharp threshold for the linear creep is an expected behavior in Maraging because its precipitates, which are all very similar to each other, do not interrupt the iron martensitic structure. The transition happens when there is sufficient stress in the material to allow dislocations to jump over the precipitates. As soon as the critical stress is reached, all dislocations can jump over all precipitates and move freely across the entire grain. The material is expected to switch from very elastic to very plastic. The sudden observed threshold is therefore an indication of the very good and uniform characteristics of the Maraging steel used.

The very limited slippage imposed on our sample is not expected to spoil the characteristics and behavior of the material.[3]

To cross check that the bake-out process has indeed burned out the creep, we then returned at 40°C and performed a long (120 day) stability measurement (Figure 7). Linear fits to the data are compatible with zero slope, i.e. no detectable creep.

All of the above measurements were performed on blades bent to a 0.0047 surface strain, corresponding to a conservative 680 MPa stress (using Maraging's 145 GPa Young's modulus).

[3] Of course any real-life creep relieving procedure would be designed to maintain the metal well below the plastic transition and thus avoid any danger of plastic slippage.

Figure 7: Long term stability check. The two curves show the same data histogrammed as raw data (left) and after applying to the data our best correction for the Young's modulus thermal change and for other external variables. The corrections are obtained using the information of auxiliary thermometers, and do not change the substance of the results.

The fits in the two curves, -0.11 +/-0.1 mm/day for the raw data and 0.15 +/- 0.1 mm/day for the corrected data are both compatible, within our measurement errors, with no creep.

4. Creep Tests At Higher Strain

A separate creep test, performed at various stress levels, including much higher stress, was performed in 2000. A number of triangular Maraging blades of different size and thickness were used in that earlier experiment. The bases of the blades were fastened at 45^{o} on the sides of a stand. Masses were loaded at the tip of each blade to bend it parallel to the floor. The triangular shape of these unconstrained blades insures constant curvature, and hence constant stress. The sizing of the individual blades was chosen to get the progression of stresses listed in Table 2, column 2. The thermal environment was a room-size, forced circulation enclosure where the temperature could be set at any temperature up to 100^{o}C with a precision of 0.020 ^{o}C/week. The forced air circulation was also inducing rapid thermalization of the blades. The droop of the blade tips was measured with Linear Variable Differential Transformer (LVDT) position sensors, continually read-out at several kHz, and the averaged droop measurements were saved at 40 s intervals. This averaging washed out the random oscillation of the blades around

their equilibrium position induced by the forced air circulation. The experiment involved baking cycles as high as 80°C, each with typical durations of 2 weeks.

This was a much more complex experiment, and potentially more sensitive than the one described in Section 2 [18]

Figure 8: Example of creep (Arbitrary Units) at 30°C (<day 20), 40°C (21<day<37) and 45°C (day>37). The line width of the logarithmic fit performed over the period between day 21 and day 36 completely covers the data points.

The experiment partially failed due to data acquisition failure (an automatic recalibration of the Data Acquisition 0 V baseline, happening at random times, corrupted data of long time baseline measurements at low creep speed), one example of which is visible in Figure 9. This failure is the reason we avoided using electronics readouts in the GAS spring tests of Section 2. The creep data was also polluted by the shrinking of the nylon LVDT coil supports as it lost its water content during the baking and possibly by small earthquake triggered changes of verticality of the pillar supporting the blades and by material hysteresis. Most of the data was eventually discarded because of these factors. The experiment was slated for repeat with new data acquisition cards from different manufacturers, peek LVDT supports, new blades, and stiffer footing, but was never run for lack of manpower.

In July 2007, that experiment was dismounted and the blades unloaded and measured. The post mortem measurement data is reported in Table 2. Some blades were found to present a rather uniform permanent bend (blades 3, 4 and 9), indicating that they

underwent large creep. The blades that underwent sizeable creep were found to have a low Rockwell hardness, indicating faulty precipitation process or poor material. Since the precipitation process was performed at the same time on all 8 blades, and all the faulty blades have the same thickness and come from the same stock, we concluded that that sheet was either not well factory solubilized prior to our precipitation process (100 hours at 435^{o}C), or it was a mislabeled, different material.

Significantly, the most stressed (1.5 GPa) blades showed no sign of permanent bend (within the original blade flatness), indicating that no significant creep had happened over the several weeks at different temperatures, including 2 weeks at 80^{o}C and the 7 years at room temperature, a result in accord with the rest of the collected data.

Table 2: Blades recovered from Totem experiment.

These measurements show that well precipitated Maraging steel can withstand much more aggressive stress than what was applied in the cantilever blades used in HAM SAS, TAMA SAS, Advanced LIGO multiple pendula, and other systems. The measurements measured no anomalous creep up to 1.5 GPa, and up to 80^{o}C. This stress level is quite close to the limit stress of 1.8 GPa measured at room temperature by Feng Gutong et al. [20] with Maraging wires hardened with this same precipitation process.

The observed failure of blades 3, 4 and 9 illustrate the importance of performing Rockwell Hardness tests on all Maraging blades before implementation, to ensure that the material has reached its design characteristics.

5. Evaluation of the Arrhenius thermal creep rate acceleration.

The difficulty of estimating the Arrhenius thermal creep rate acceleration is to distinguish, during temperature transients, the relatively small variation of creep speed against the background of the much larger effects induced by the thermal variations of Young's modulus. We used some of the first experiment data when the creep was still fast and data corruption was not yet very significant and still under control. The final evaluation is the fruit of a long and progressive reduction of the error fork using several arguments.

Initially, we compared the creep speed change around the first temperature transient data (between 30°C and 40°C) of the six blades available at that time.

We used the creep plot themselves to evaluate the thermal transient time. We determined that the thermal transient started at hour 98.4, and that the blade had reached thermal equilibrium by hour 120. We also applied linear fits to the data segments before the transient and after hour 120. The ratios of the slopes before and after the transient (Figure 9) were used as the measurement of the ratio of the actual creep speeds at the two temperatures. By ignoring the 20 hours during the temperature switch, we forfeited measurement of the initial phases thus underestimating the second slope and possible detection of any fast creep component that may be generated at the beginning of the thermal transient.

Figure 9. Creep slope evaluation for a blade, before and after a 10°C temperature raise. The linear fit before hour 98.4 and after hour 120 gave slopes of 0.00026 and 0.0016

respectively. The slope ratio of 6.11, from the fits in this figure, is the highest measured over the 6 blade measurements available. One of the DAQ jumps that eventually corrupted the long-term measurement is visible at about hour 115.

An average over the slope ratios of the fits performed on the available blades (slope ratios: 5.11, 4.95, 5.3, 6.11, 4.8, 5.16, 3.7) gave a mean of 5 +/-0.3, corresponding to a creep speed acceleration of 1.175/^{o}C. This statistically seemed to promise a good quality measurement. The problem is that by waiting out the transient, the second slope is under-evaluated. In theory, this under-evaluation can be corrected by fitting the data with a logarithm function, and back extrapolating the slope to the moment just after the thermal transient.

To attempt to determine this time, exponential fits to the data accounting for the thermalization in addition to a logarithmic function for the creep were performed. The fits, one of which is shown in Figure 10, were of good quality. We found exponential thermalization constants of roughly 1.5 hours, reasonably consistent between all blades and with the air thermalization times in the enclosure. The exponentially fitted component of the droop was then subtracted from the data. The critical question was to (arbitrarily) decide how many thermalization time constants to wait for before picking the slope from the logarithmic fitted component of the data. The thermalization times, despite the forced air circulation, are still too large for a meaningful determination of the correction factor.

This indetermination yielded a correction factor of the order of 4, varying by a factor of 2, which is clearly an unsatisfactory result.

Figure 10: Exponential and logarithmic fit to a thermal transient data set.

Having failed to effectively use the data of an up-step of temperature, we modified the original data gathering strategy, generated a temperature down-step and analyzed its data. In a logarithmic function, the second derivative is $1/t^2$, drops faster than the slope itself (1/t). In a temperature down-step, the error in extrapolation and the determination of the slope after the transient should be depressed.

This measurement was performed at 45°C, lowering the temperature to 40°C. A small (5°C) temperature step was chosen to obtain a still measurable slope at the lower temperature. From an average over several blades, we obtained a creep speed variation of

$$\frac{\sigma_{40^\circ C}}{\sigma_{45^\circ C}} = 0.202 \pm 0.025$$

In this analysis we realized that we had run into a different, but even more serious problem.

For about 7 to 8 days after the temperature drop (well beyond the several hours time scale of the Young's modulus variation effects) the creep data streams of all blades showed flat or negative curvature instead of the positive curvature expected from a logarithmic behavior. Only in the second week did the creep resume its normal logarithmic characteristic.

Figure 11

Figure 11 zoomed

Figure 11: Transient from 50°C to 45°C and up to 60°C and zoom on the 45°C region. For a week after the temperature change, the creep graph curvature was inverted. This effect, common to all blades, is better visible on the zoomed image, in which the vertical scales of several blades have been shifted to illustrate the common behavior. Thermal variation of the Young's modulus does not explain this effect, which supposedly may be due to material hysteresis. Note that the temperature shown in the graph is shifted by 2°C with respect to the temperature of the PID controller, reported in the text. This difference between the two thermometers was stable to a few m°C level and has no effect in any of the measurements reported.

We attributed this anomalous behavior to hysteresis in the blades (the effects of hysteresis were eliminated in the GAS filter experiment of Section 2 by the excitation of the vertical oscillation of the blades as discussed in reference [21]).
We therefore fell back on a third method.
We considered the end slope at the end of each of the following four baking period in the 30°C to 40°C and in the 50°C to 45°C. We chose these periods because they have the same time length. The end slopes are supposedly far from either Young's modulus and hysteresis transient perturbations. In the 30°C to 40°C temperature change, the initial slope of the 40°C period is clearly underestimated, while in the 50°C to 45°C temperature change, the initial slope of the 45°C period is clearly overestimated.

We can therefore safely use these two data sets to generate a lower and a higher limit of the thermal creep speed acceleration.

Table 3: Evaluation of upper and lower limit of the Arrhenius thermal creep speed acceleration.

From this data we determined an Arrhenius acceleration of 1.28±0.13/^{o}C.

From the measured Arrhenius acceleration of the drift speed change one can estimate the activation energy E_{act} of the dislocations responsible for creep. Maraging (and all crystalline metals in general) have a very large pool of dislocations. Some, uninteresting, are completely pinned down, some are sitting against precipitates and stick to them with various binding energies, depending on the type of dislocation and precipitates. Of these, the ones with activation energies below or near thermal energies (kT) are completely free to move, and can contribute to hysteresis. The dislocations that induce creep are the unstable ones with binding energies much above kT (of course only the dislocations sitting against precipitates on the downslope of the stress field can gain energy in moving and are unstable.). These can be activated only by large local fluctuations of thermal energy. The probability that a thermal fluctuation is large enough to reach up to E_{act} can be written as $e^{-\frac{E_{act}}{KT}}$. The creep speed σ can then be written as the product of a slowly varying constant a(t) (proportional to the number of the remaining available dislocations, which are slowly used up in the creep process; a(t) has logarithmic behavior to reflect the

progressive depletion of the available dislocation pool) times the mean dislocation thermal activation probability. The creep speed has then the form $\sigma = \alpha(t) \bullet e^{-\frac{E_{act}}{KT}}$. Using the creep speed measurements before and after a sudden temperature change, we obtain:

$$\sigma_1 = \alpha(t) \bullet e^{-\frac{E_{act}}{KT_1}}$$

$$\sigma_2 = \alpha(t) \bullet e^{-\frac{E_{act}}{KT2}}$$

$$\ln\frac{\sigma_1}{\sigma_2} = \frac{E_{act}}{KT_2} - \frac{E_{act}}{KT_1} = E_{act}\frac{T_1 - T_2}{KT_1T_2}$$

$$E_{act} = \frac{KT_1T_2}{T_1 - T_2}\ln\frac{\sigma_1}{\sigma_2}$$

$$E_{act-\max} = .86 \bullet 10^{-4} \bullet 303 \bullet 313 \bullet \ln(1.139) = 1.06eV$$

$$E_{act-\min} = .86 \bullet 10^{-4} \bullet 318 \bullet 323 \bullet \ln(1.413) = 3.05eV$$

$$E_{act} = 2.(\pm 1.)eV$$

6. Measurement of the thermal variation of the Young's modulus

The thermal variation of the Maraging Young's modulus was made in two ways.

In the first method the thermal change of the spring lifting power was measured from the data of Table 1, column 3, when returning to a lower temperature level. This estimation was not made on the up-transients to higher temperature levels to offset the effects of creep.

Only the transients from 40 to 30°C, from 60 to 40°C and from 90 to 40°C were used (Table 4) because for higher temperature steps changes in payload were required.

The thermal droop was transformed in lifting power change using a position versus load data previously gathered at 30°C.

Table 4: Determination of the thermal change of the Young's modulus.

A weighted average of the three data points yielded a value of $2.16(\pm 0.07) \times 10^{-4}/^{o}C$ for the thermal change of the Young's modulus.

An independent determination of the thermal change of the Young's modulus was performed with a virtually identical GAS filter during the course of a separate experiment [6]. This filter was equipped with a coaxial LVDT position sensor and a voice coil actuator. A feedback between the sensor and the actuator with a 1000 second time constant integration filter was used to maintain the vertical position of the filter at its working point while the ambient temperature changed between 22.5 and 23°C.
The voice coil current was monitored as a measurement of the correction force necessary to compensate for the change of Young's modulus. The voice coil force versus current slope was measured by adding known masses on the payload and noting the jumps in feedback current on the actuator. The data thus calibrated is shown in Figure 12. The fit gives a value of $2.20 \times 10^{-4}/^{o}C$ for the thermal change of the Young's modulus with a 0.25% statistical error on the fit, a 0.3% error in the payload determination, and a similar error in the voice coil calibration. Adding up in quadrature these three errors, we get a 0.5% error on the measurement, i.e. $2.2170(\pm 0.011) \times 10^{-4}/^{o}C$.

Combining the two measurements, which marginally agree within their errors, we obtain 2.203 (±0.013) x 10^{-4}/°C.

Figure 12: Correction force necessary to maintain the GAS spring at its working point as temperature changes.

7. Conclusions

We measured creep in stressed Maraging blade springs over extended periods of time and different temperatures. We observed a creep of 0.44% of the original blade bending. Similar creep levels can be expected over the years in any system made with loaded Maraging blades. Simply baking the blades under their nominal stress can eliminate the creep effects.

We measured a thermal variation of the Young's modulus of 2.023 (±0.013) 10^{-4}/°C.

We estimated an Arrhenius thermal variation of creep speed of 1.28±0.13/°C and a dislocation activation energy of $E_{act} = 2.0(\pm 1.0)eV$.

Including the Arrhenius acceleration factor, we achieved spring ageing of 100 billion years. We verified that no residual creep is detectable after this heat treatment.

We found that blades stressed at 680 MPa presented normal logarithmic creep up to a temperature of 190°C, but experienced linear runoff creep at 200°C.

Well hardened blades, stressed up to 1.48 GPa, did not show any excess creep up to temperatures of 80°C.

Acknowledgements

In memory of Michael Koyfman, he gave us a great example of friendship and courage.
We would like to thank the National Science Foundation which granted for the SURF program, Caltech and the SURF office.
Some of the authors visited the LIGO laboratories at Caltech within the framework of a summer student exchange program between the LIGO project at Caltech and INFN.
The LIGO Observatories were constructed by the California Institute of Technology and Massachusetts Institute of Technology with funding from the National Science Foundation under cooperative agreement PHY 9210038. The LIGO Laboratory operates under cooperative agreement PHY- PHY-0107417. This paper has been assigned LIGO Document Number LIGO-P070095-00-Z.

References

[1] The creep problem in the VIRGO suspensions: a possible solution using Maraging steel., M. Beccaria, . . . , V. Rubino, et al., Nuclear Instruments & Methods in Physics Research, 1998, vol. 404, no 2-3, pp. 455-469

[2] Riccardo DeSalvo, "Non-stochastic noise in gravitational wave detectors", second Edoardo Amaldi conference on Gravitational waves, CERN Switzerland, 1-4 July **1997** World Scientific Publishing Co, P.O. Box 128 Farrer Road, Singapore 912805, page 228-239, LIGO Document No. P970036-00-D, available at http://admdbsrv.ligo.caltech.edu/dcc/

[3] G. Cella “Monolithic geometric anti-spring blades” Nuclear Instruments and Methods in Physics, Volume 540, Issues 2-3, 21 March 2005, pp. 502-519

[4] DeSalvo, R., et al., 1997–1999, “Performance of an Ultra-Low Frequency Vertical Pre-Isolator for the Virgo Seismic Attenuation Chains,” Nucl. Instrum. Methods Phys. Res. A, **420**, pp. 316–335.

[5] Cella, G., et al., 2002, “Seismic Attenuation Performance of the First Prototype of a Geometric Anti-Spring Filter,” Nucl. Instrum. Methods Phys. Res. A, **487**, pp. 652–660.

[6] Mantovani, M., and DeSalvo, R., 2004, “One Hertz Seismic Attenuation for Low Frequency Gravitational Waves Interferometers,” Nucl. Instr. and Meth., Volume 554, Issues 1-3, 1 December 2005, pp. 546-554

[7] A. Bertolini, et al., “Design and prototype tests of a Seismic Attenuation System for the Advanced-LIGO Output Mode Cleaner”, Class. Quantum Grav. 23 (2006) S111–S118 LIGO document LIGO-P050024-00-D, available at http://admdbsrv.ligo.caltech.edu/dcc/

[8] Alberto Stochino, Doctoral thesis, Dipartimento di Fisica “Enrico Fermi”, Universitá di Pisa, Largo Bruno Pontecorvo, I-56127 Pisa, July 2007, LIGO Document No. P070083, available at http://admdbsrv.ligo.caltech.edu/dcc/

[9] Beccaria, M., et al., 1997, “Extending the Virgo Gravitational Wave Detection Band Down to a few Hz, Metal Blade Springs and Magnetic Antisprings,” Nucl. Instrum. Methods Phys. Res. A, **394**, pp. 397–408

[10] DeSalvo, R., et al., 1997–1999, “Performance of an Ultra-Low Frequency Vertical Pre-Isolator for the Virgo Seismic Attenuation Chains,” Nucl. Instrum.

Methods Phys. Res. A, **420**, pp. 316–335.

[11] Riccardo DeSalvo, "Passive, Nonlinear, Mechanical Structures for Seismic Attenuation", Journal of Computational and Nonlinear Dynamics CND-05-1090, In press, October 2007

[12] A New Seismic Attenuation Filter Stage MGASF For Advanced Gravitational Wave Interferometric Detectors, V. Sannibale, A. Bertolini, G. Cella, R. DeSalvo, S Ma`rka, K. Numata}, A.Stochino, A Takamori, H. Tariq, to be Submitted to NIM-A

[13] (ref. Maraging steel has been used in this super-plastic regime as a damping material to absorb the rocket vibration in the Apollo capsule seats, private communication, David Platus, Minus K Technology, 420 S. Hindry Ave., Unit E Inglewood, CA 90301, http://www.minusk.com)

[14] A. Takamori, "Low Frequency Seismic Isolation for Gravitational Wave Detectors", Doctoral Thesis, University of Tokyo (2003) LIGO Document No. P030049, available at http://admdbsrv.ligo.caltech.edu/dcc/

[15] Takamori, A., et al., 2002, "Mirror Suspension System for the TAMA SAS," Class. Quantum Grav., **19** pp. 1615–1621.

[16] Marka, S., et al., 2002, "Anatomy of the TAMA SAS Seismic Attenuation System," Class. Quantum Grav., **19**, pp. 1605–1614.

[17] Nicole Virdone, et al., Preliminary results from the measurement of creep in Maraging blades LIGO technical note Document no. T050047-00-R, available at http://admdbsrv.ligo.caltech.edu/dcc/

[18] Rosalia Stellacci,

[19] Rosalia Stellacci, et al., "The GAS blade creep measurements, problems and some

solutions.", LIGO technical note Document no. T010112, available at
http://admdbsrv.ligo.caltech.edu/dcc/
[20] F. Gutong, S. Braccini, C. Casciano, V/ Dattilo, R. DeSalvo, F. Frasconi, G. Gennaro, R. Passaquieti, R. Valentini. CNRS, INFN, & VIRGO internal report. Ref: VIR-TRE-PIS-4600-129. June 1997
[21] DeSalvo, R., et al., 2005, "Study of Quality Factor and Hysteresis Associated with the State-of-the-Art Passive Seismic Isolation System for Gravitational Wave Interferometric Detectors," Nucl. Instr. and Meth., Volume 538, Issues 1-3, 11 February 2005, Pages 526-537.
[22] R. DeSalvo, "Passive, non-linear, mechanical structures for Seismic Attenuation", Journal of Computational and Non-Linear Dynamics", Vol 2, pag 290-298, October 2007

TABLES

Table 1: Measured creep data. The time expansion factor is obtained using creep acceleration rate of 1.174/^{o}C (corresponding to an assumed factor of 5 per 10^{o}C temperature increase). The effective ageing time (column 7) is obtained multiplying column 4 by column 6.

Cycle	Temperature [°C]	Creep Saturation level [mm]	Cycle Duration [days]	Measured creep [mm]	Time expansion (acceleration) factor	Effective ageing time in cycle [days]	Integrated effective ageing time [years]
1	30	9.28	1		3.6	3.62	9.93E-03
2	40	8.69	4	0.00	18	72.5	2.08E-01
3	30	9.17	2		3.6	7.25	2.28E-01
4	60	7.18	41	0.26	4.5E+02	1.86E+04	5.11E+01
5	40	8.43	8		18	145	5.15E+01
6	90	4.93	20	0.56	5.7E+04	1.13E+06	3.15E+03
7	40	8.13	20		18	362	3.16E+03
8	150	2.07	19	1.17	8.8E+08	1.68E+10	4.61E+07
9	40	7.52	7		18	127	4.61E+07
10	170	3.36	27	1.33	2.2E+10	5.97E+11	1.68E+09
11	40	7.36	7		18	127	1.68E+09
12	190	2.96	14	1.51	5.5E+11	7.74E+12	2.29E+10
13	40	7.18	10		18	181	2.29E+10
14	200	2.00	20	1.73	2.8E+12	5.53E+13	1.74E+11
15	40	6.96	118		18	2.14E+03	1.74E+11

1 Table 2: Blades recovered from Totem experiment.

Blade #	Stress [GPa]	Permanent bend [mm]	Rockwell A hardness	Blade thickness [mm]	Nom. Blade bending radius [mm]
1	0.735	1.5	51.8	2.97	293
2	0.735	0.50	52.0	2.97	293
3	0.824	10	30.1	3.33	293
4	0.829	7.0	30.4	3.35	293
5	0.948	0.50	52.3	3.83	293
6	0.960	0.50	51.9	3.88	293
7	1.124	1.0	52.5	2.96	191
8	1.127	1.0	52.2	2.97	191
9	1.272	21	34.0	3.35	191
10	unloaded	0	29.8	3.37	191
11	1.484	0.0	52.9	3.91	191
12	1.484	0.0	52.4	3.91	191

2

1 Table 3: Evaluation of upper and lower limit of the Arrhenius thermal creep speed

2 acceleration.

Drift speed thermal acceleration	Lower limit x/^{o}C	Upper limit x/^{o}C
Blade 1	1.1093	1.3747
Blade 2	1.1525	1.4171
Blade 3	1.1103	1.4424
Blade 4	1.1140	1.4945
Blade 5	(1.2342)	1.4310
Blade 6	1.1514	1.3356
Blade 7	1.0985	1.3488
Blade 8	1.1387	1.4572
Mean	1.139	1.413
Std Deviation	0.044	0.055

3

1 Table 4: Determination of the thermal change of the Young's modulus.

Initial T	End T	DT	Droop	Hoist power loss	Young's modulus variation	
^{o}C	^{o}C	^{o}C	mm	gram	1/^{o}C	
40	30	10	0.48	107.2	1.7	x 10^{-4}
60	40	20	1.25	279.1	2.19	x 10^{-3}
90	40	50	3.2	714.6	2.24	x 10^{-3}

2

Figure 1

Click here to download high resolution image

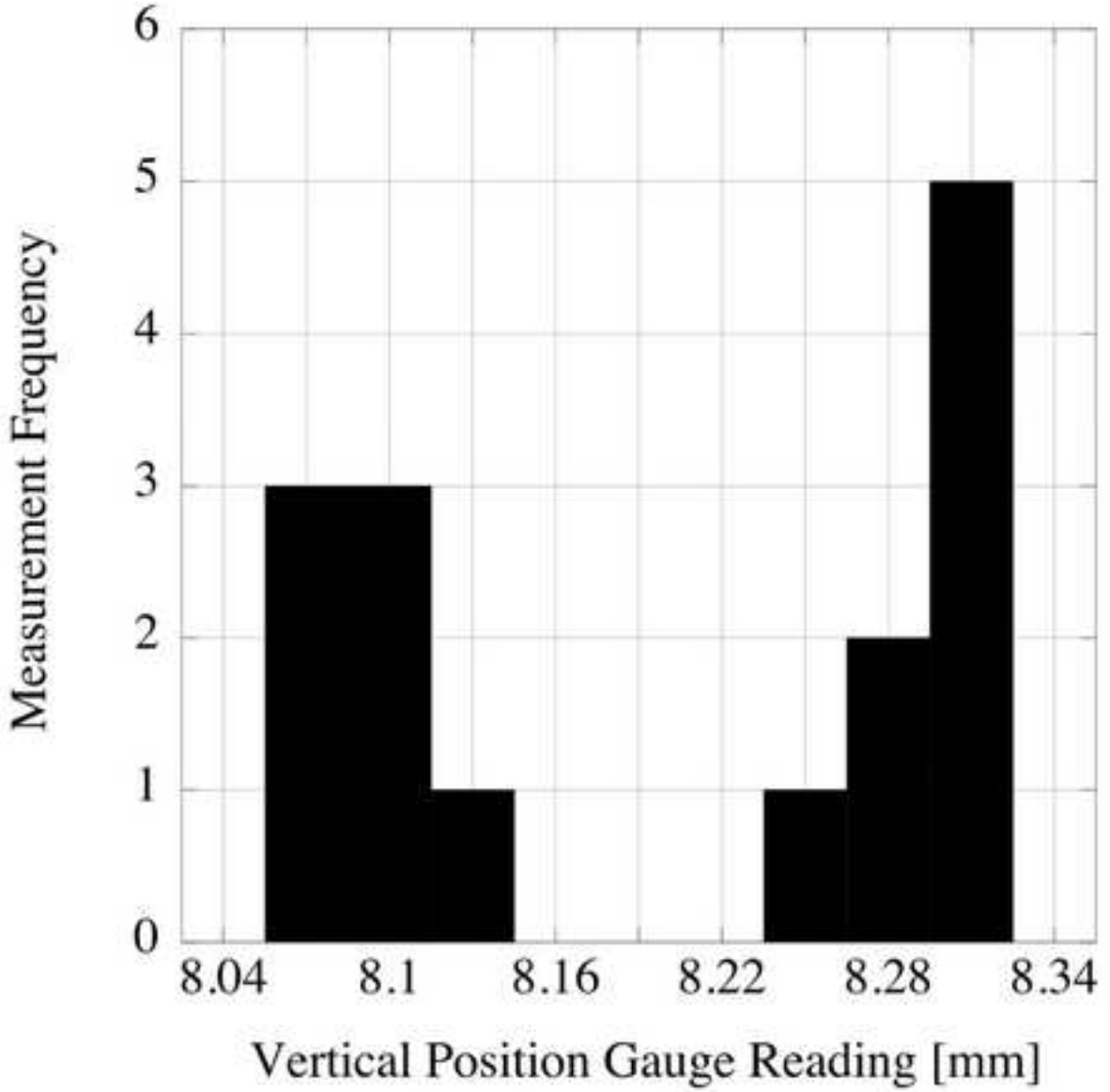

Figure 2

Click here to download high resolution image

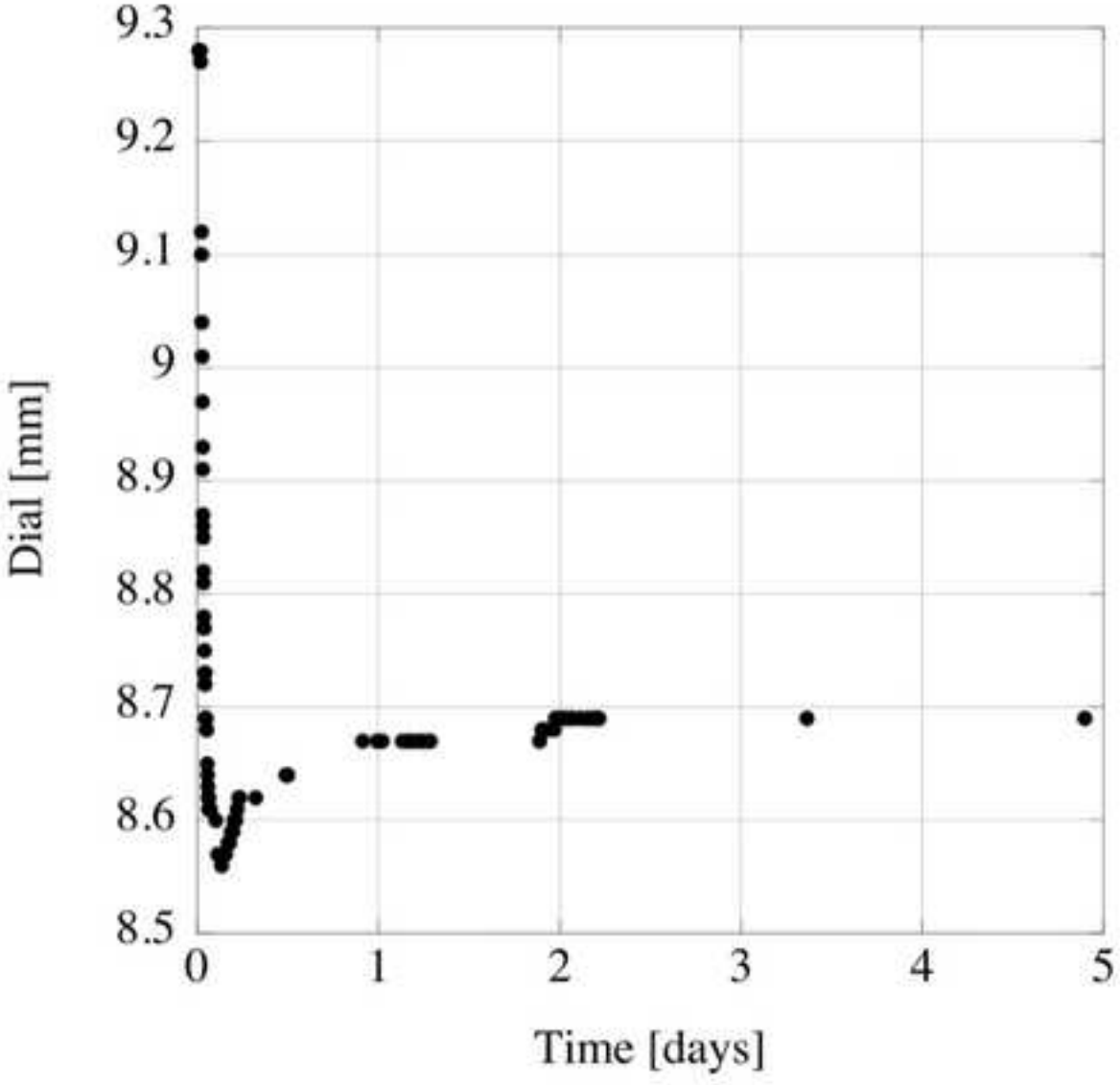

Figure 3

Click here to download high resolution image

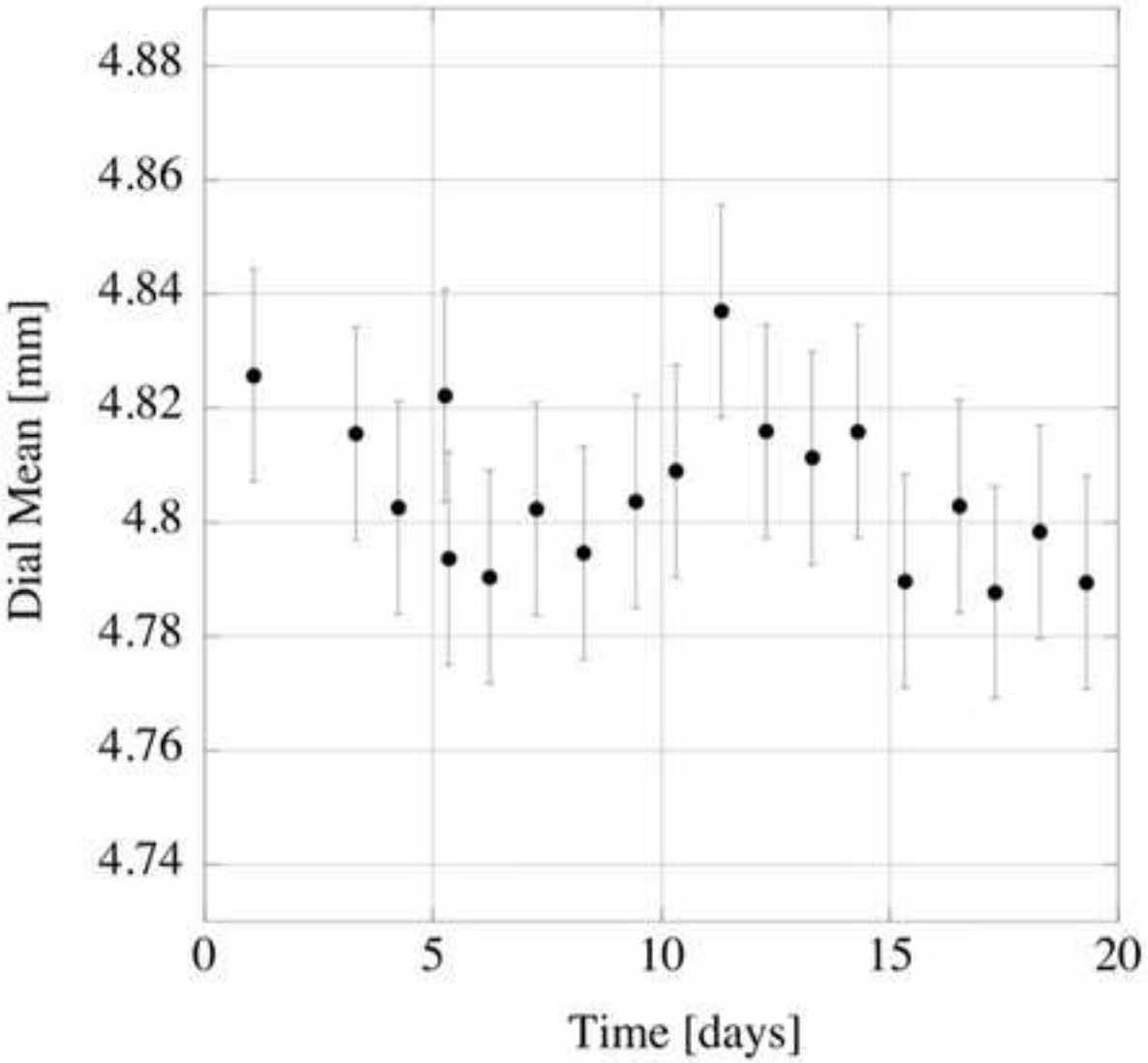

Figure 4a

Click here to download high resolution image

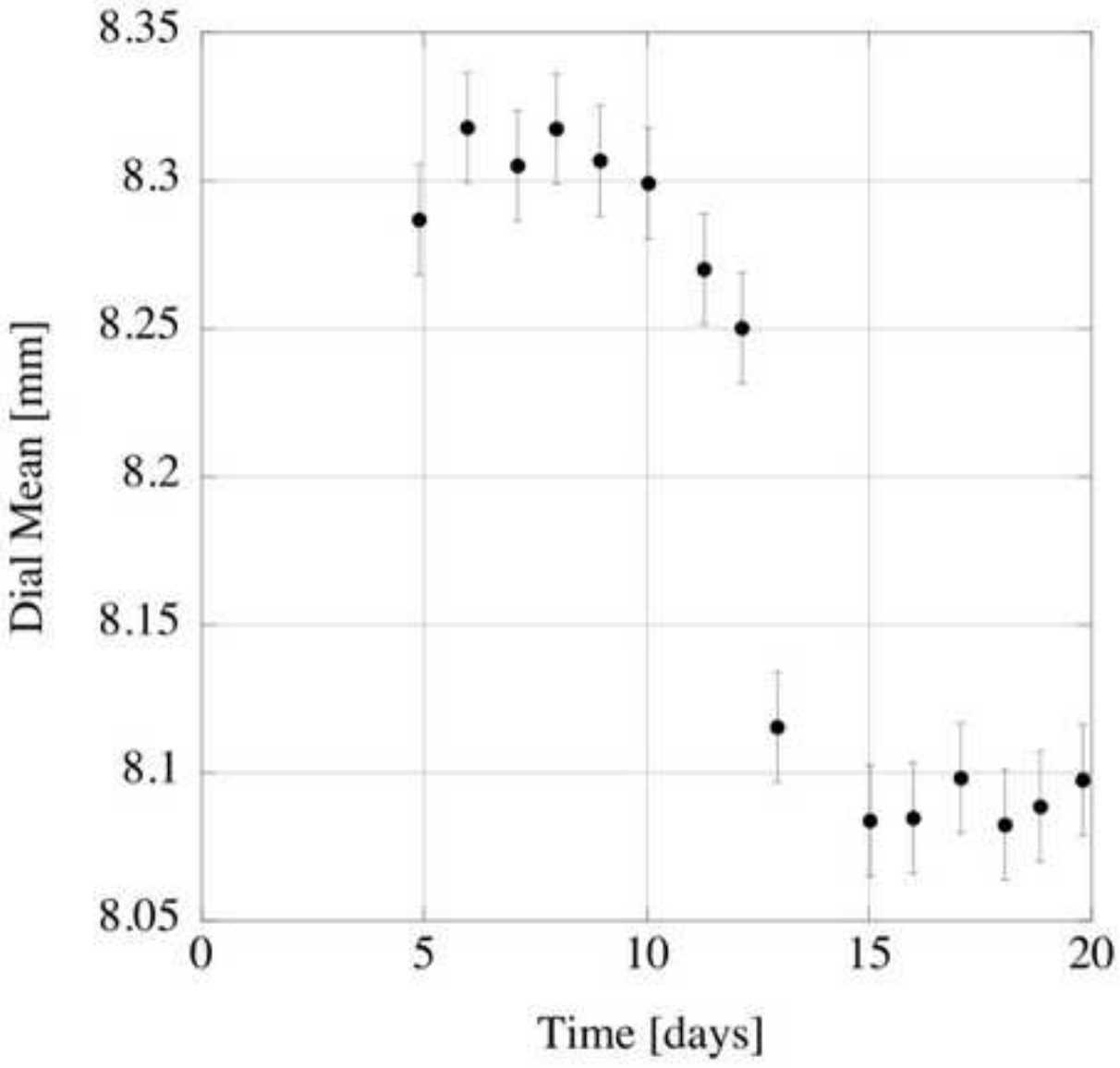

Figure 4b

Click here to download high resolution image

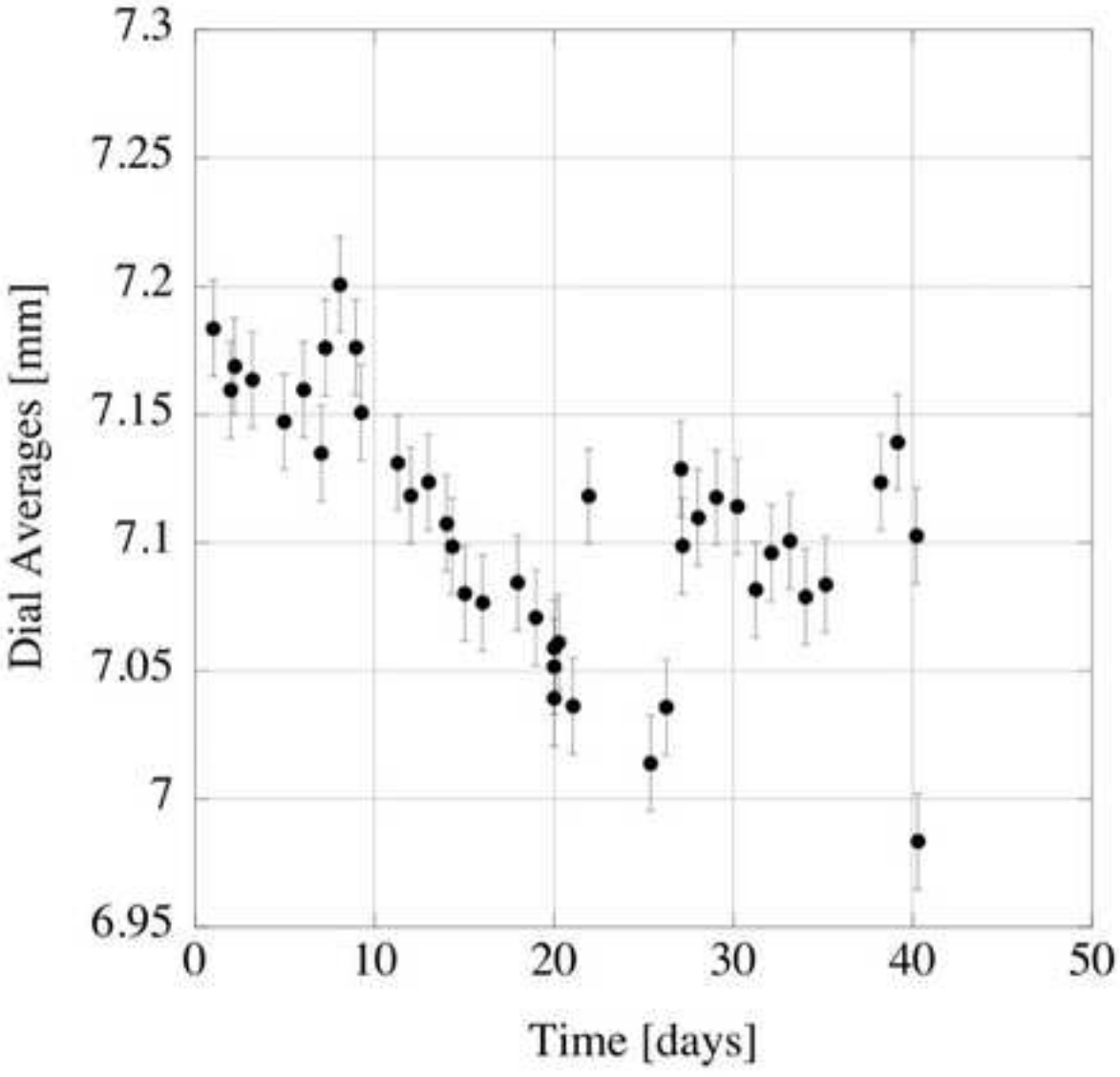

Figure 5

Click here to download high resolution image

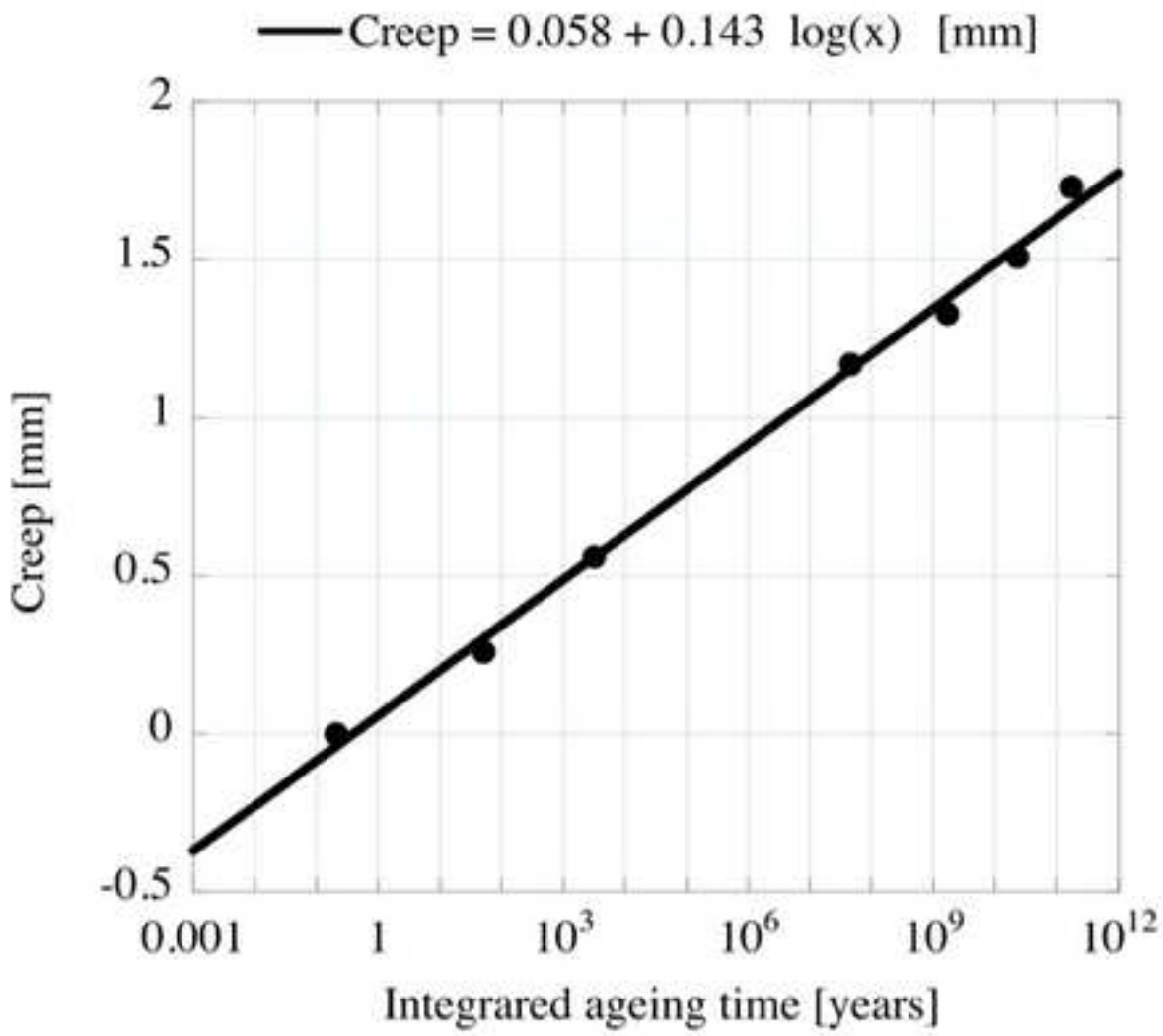

Figure 6

Click here to download high resolution image

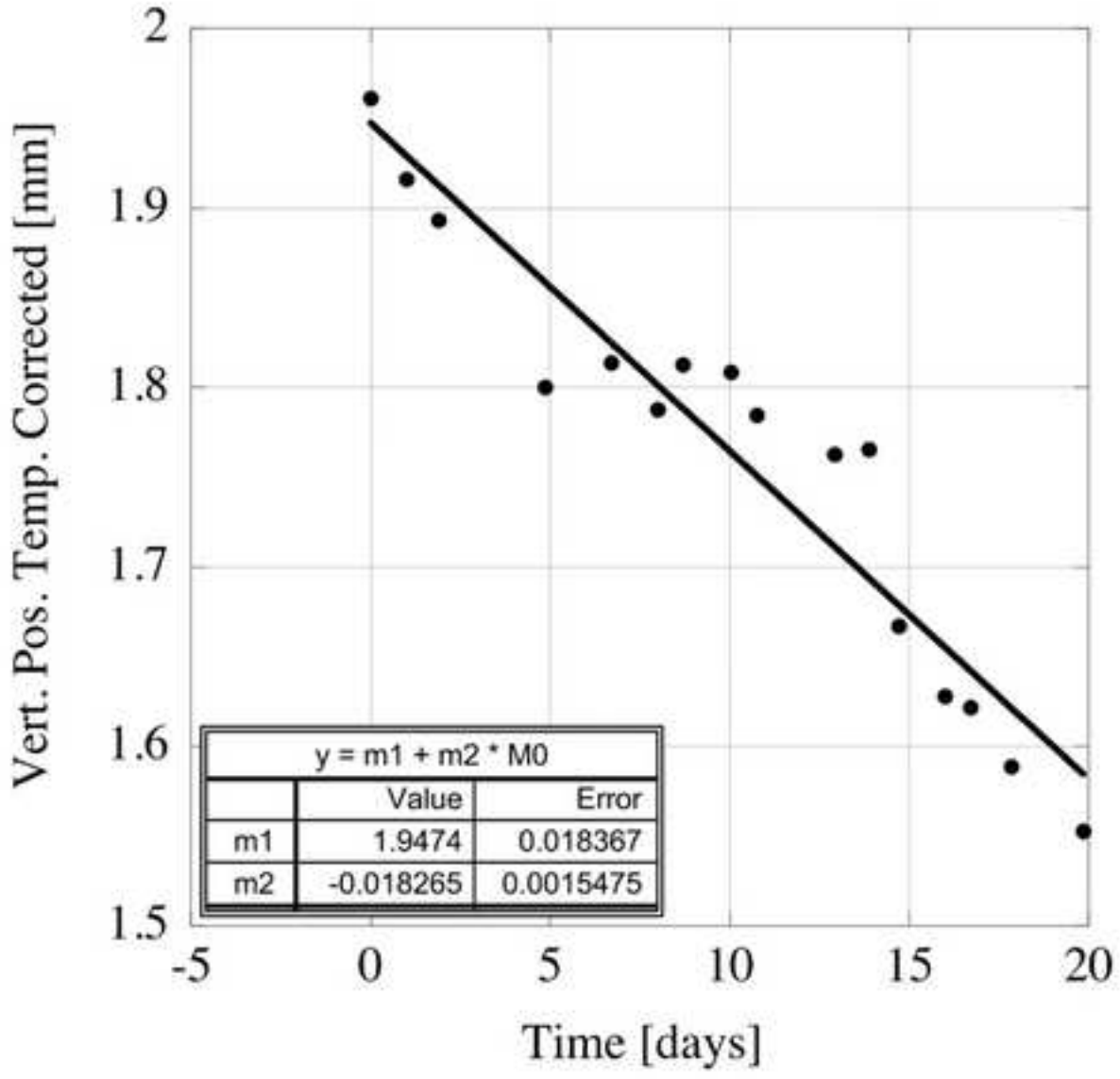

Figure 7a

Click here to download high resolution image

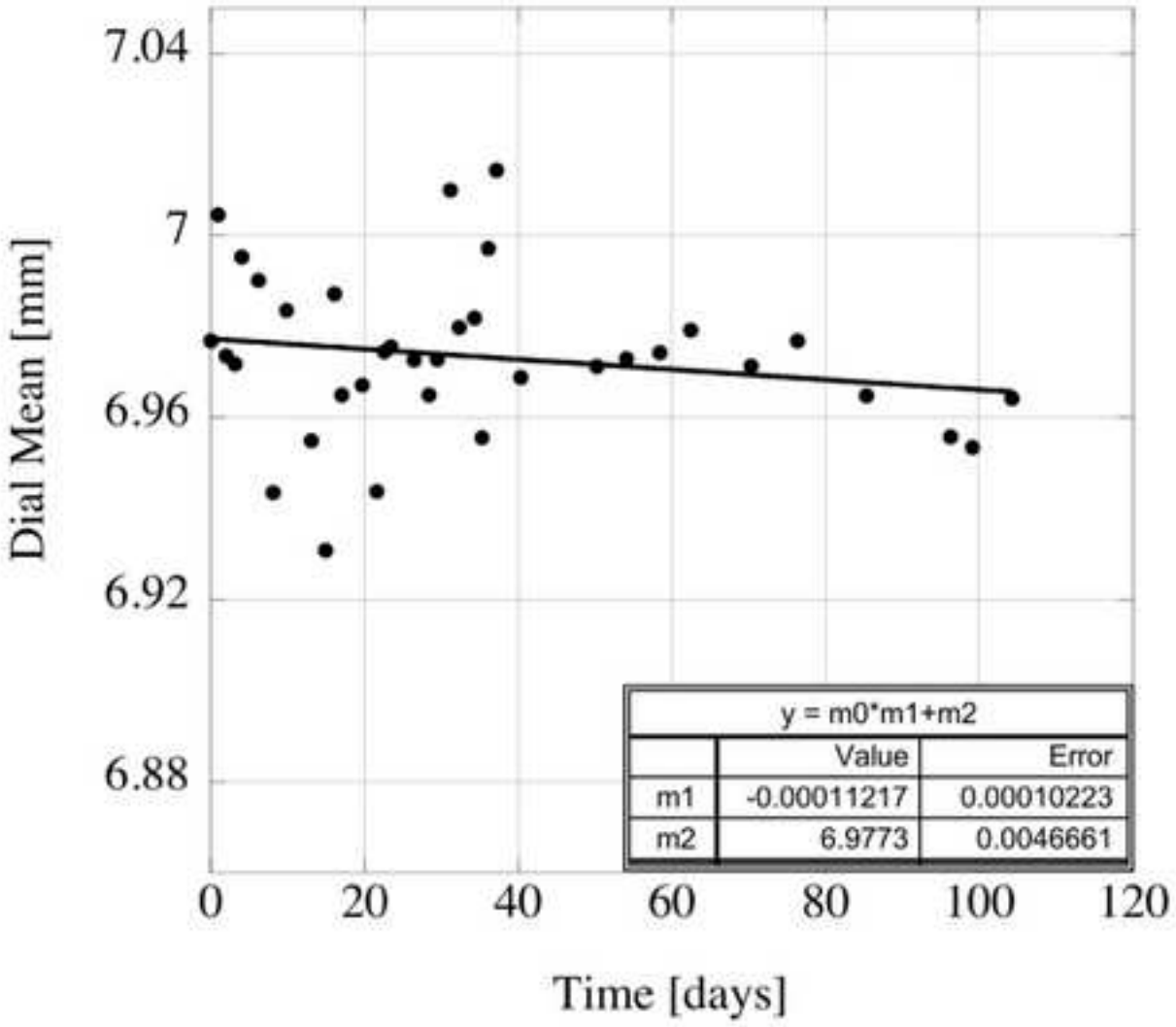

Figure 7b

Click here to download high resolution image

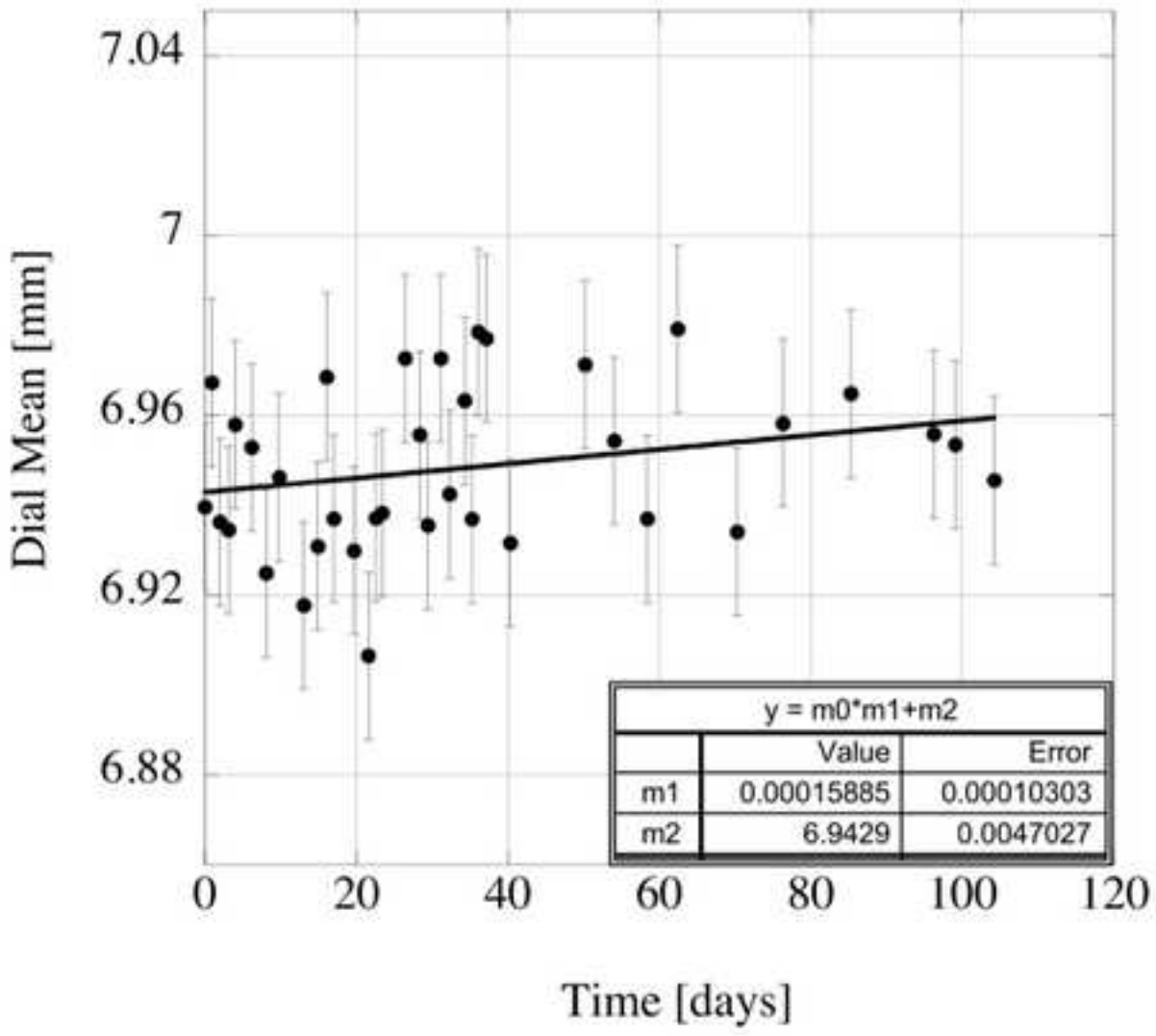

Figure 8

Click here to download high resolution image

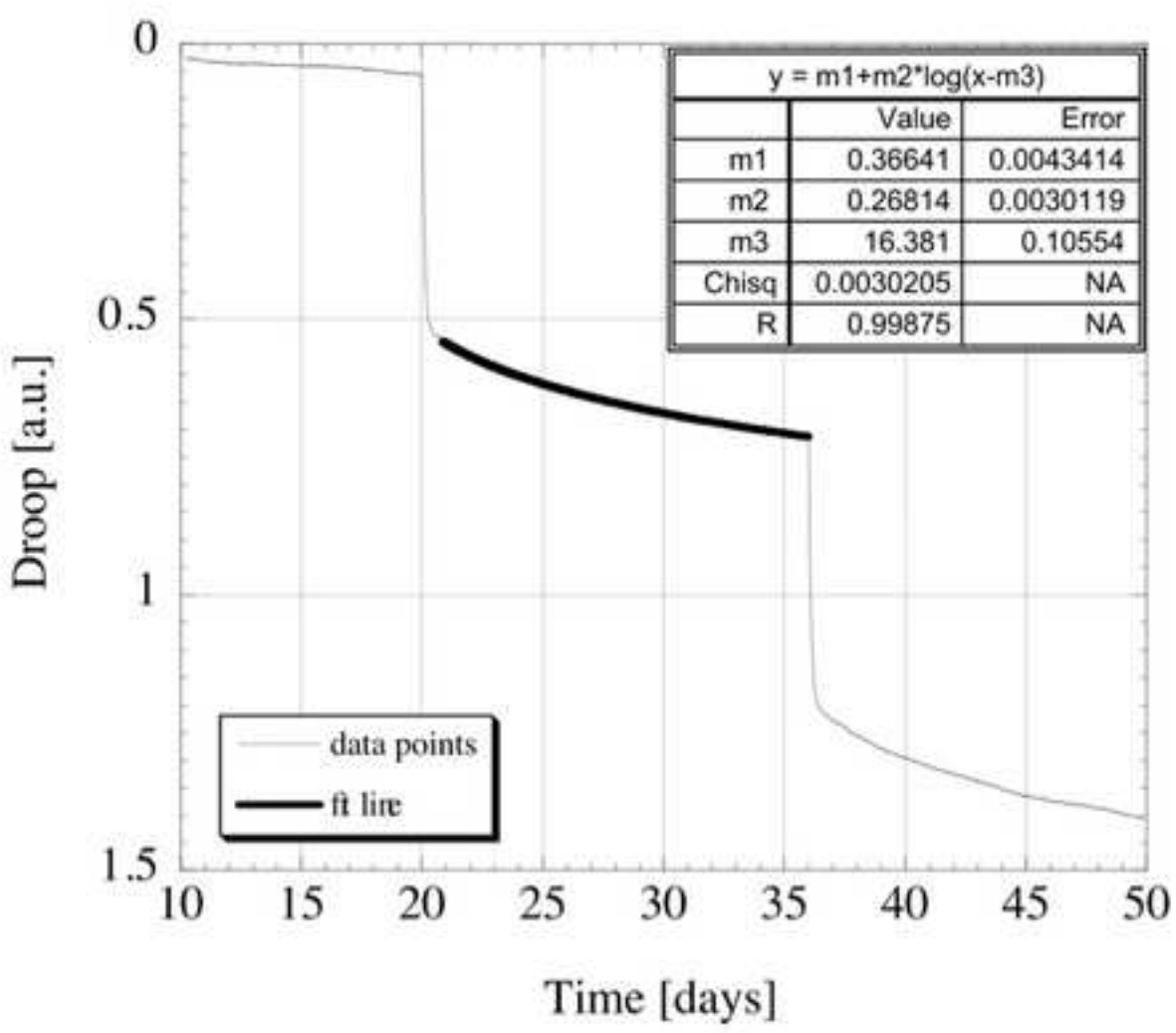

Figure 9

Click here to download high resolution image

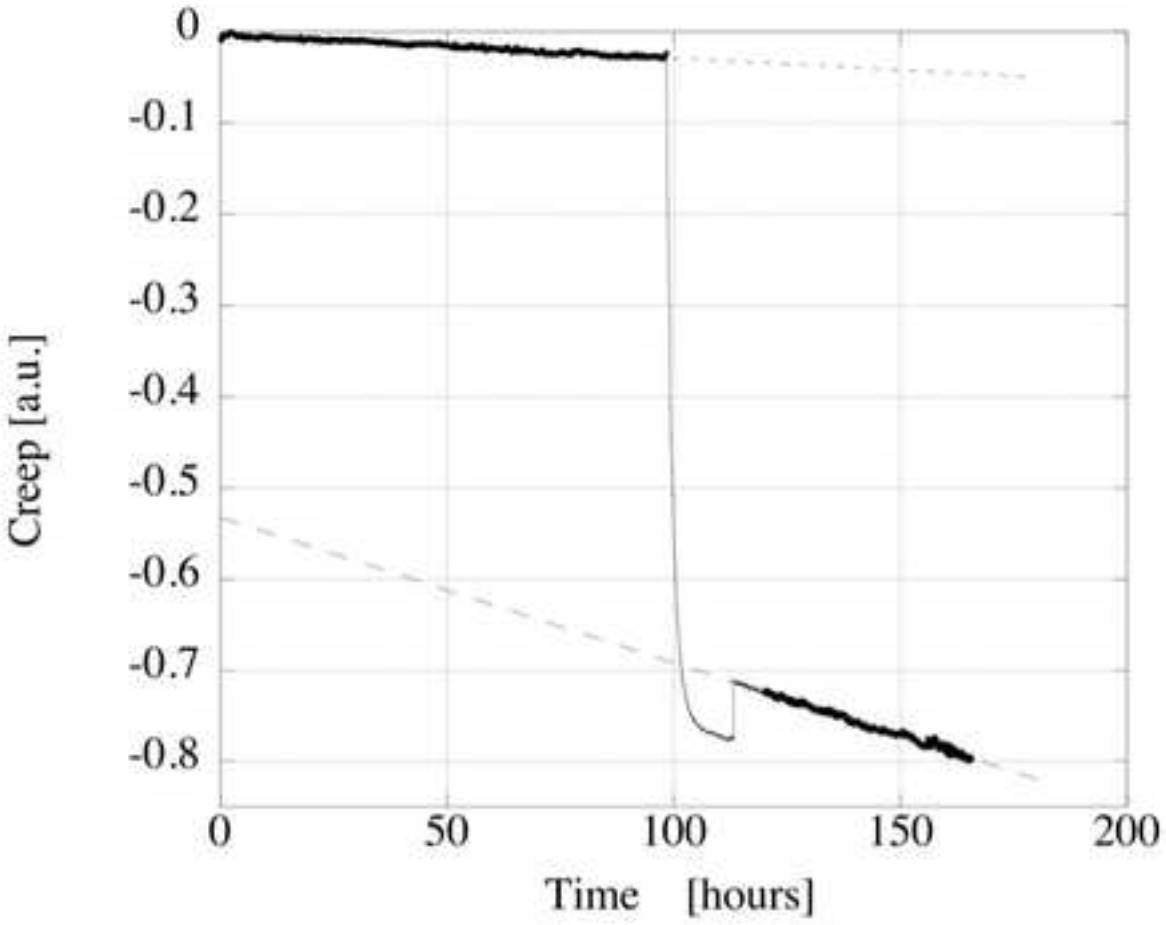

Figure 10

Click here to download high resolution image

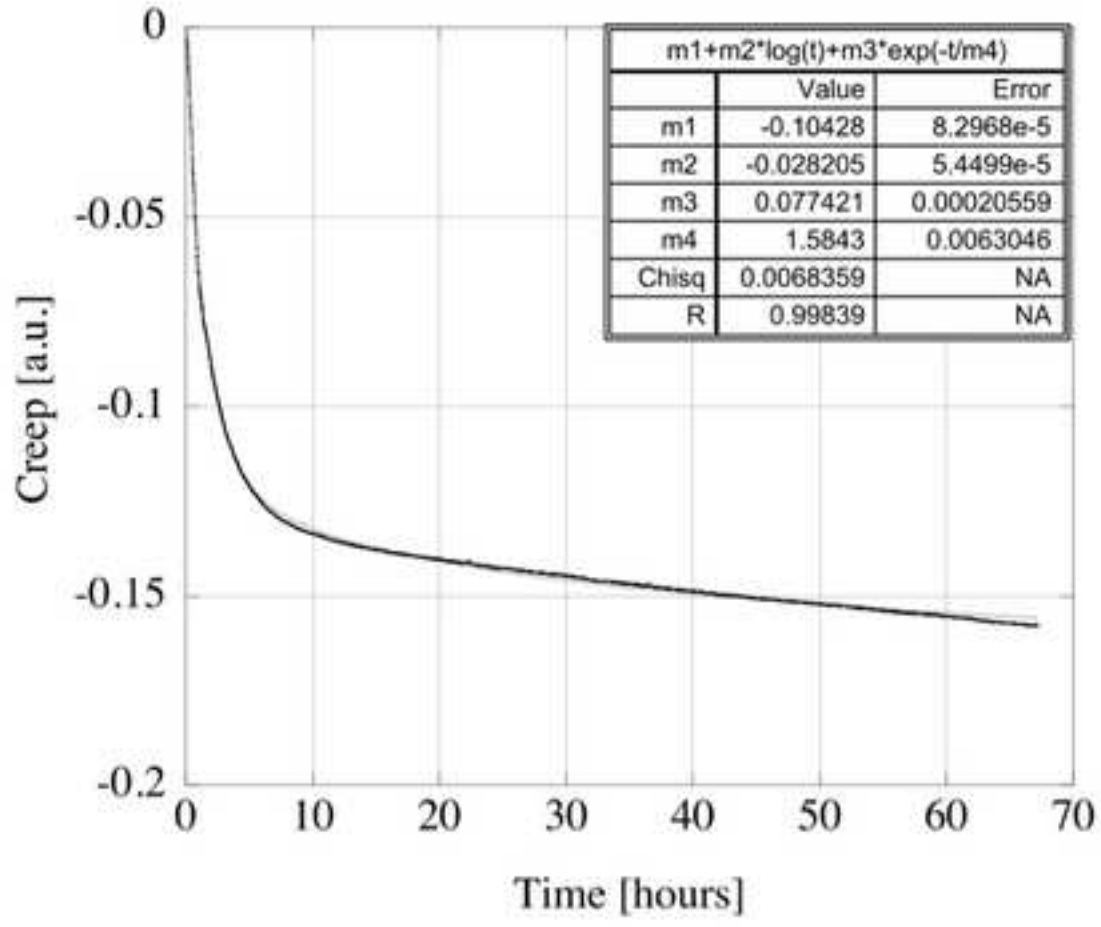

Figure 11a

Click here to download high resolution image

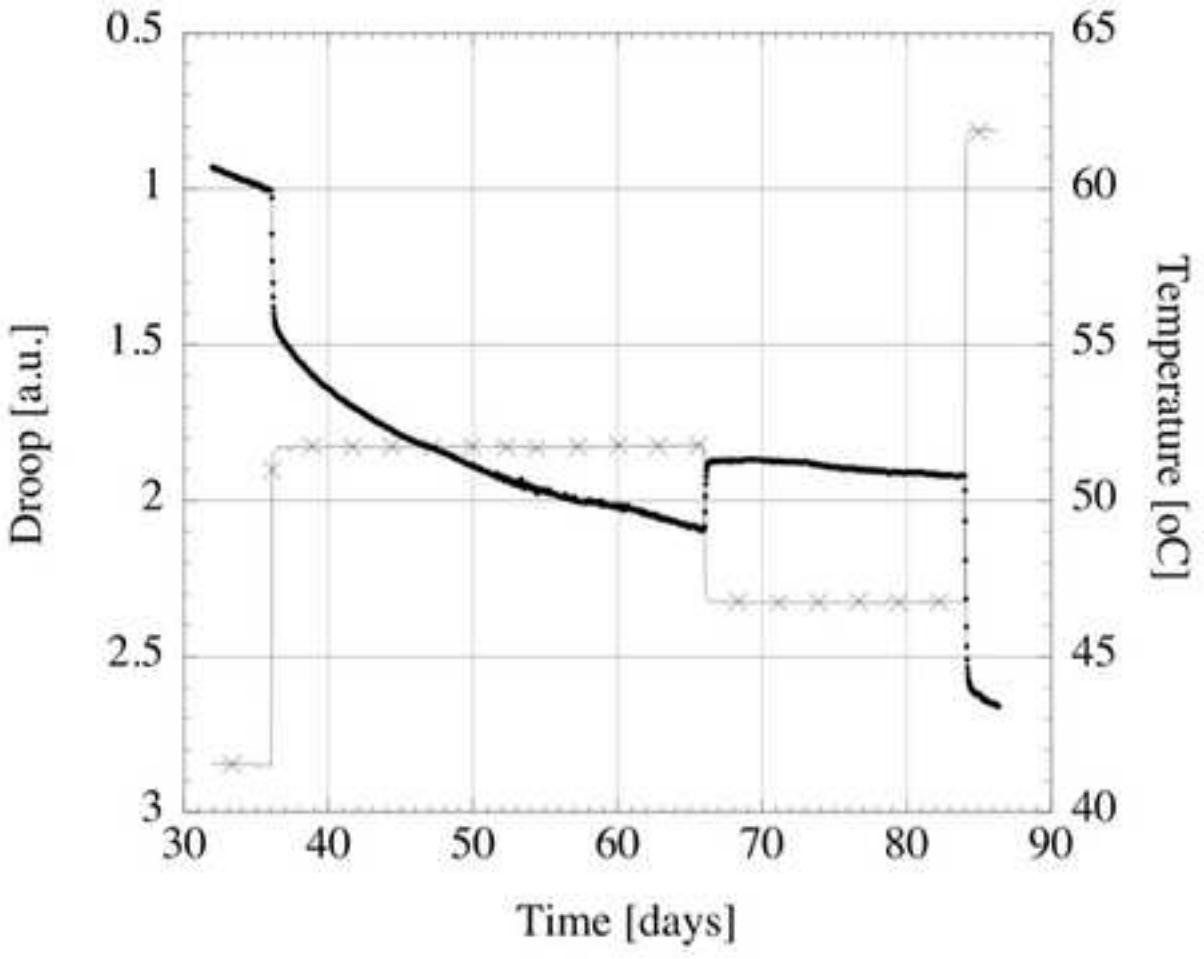

Figure 11b

Click here to download high resolution image

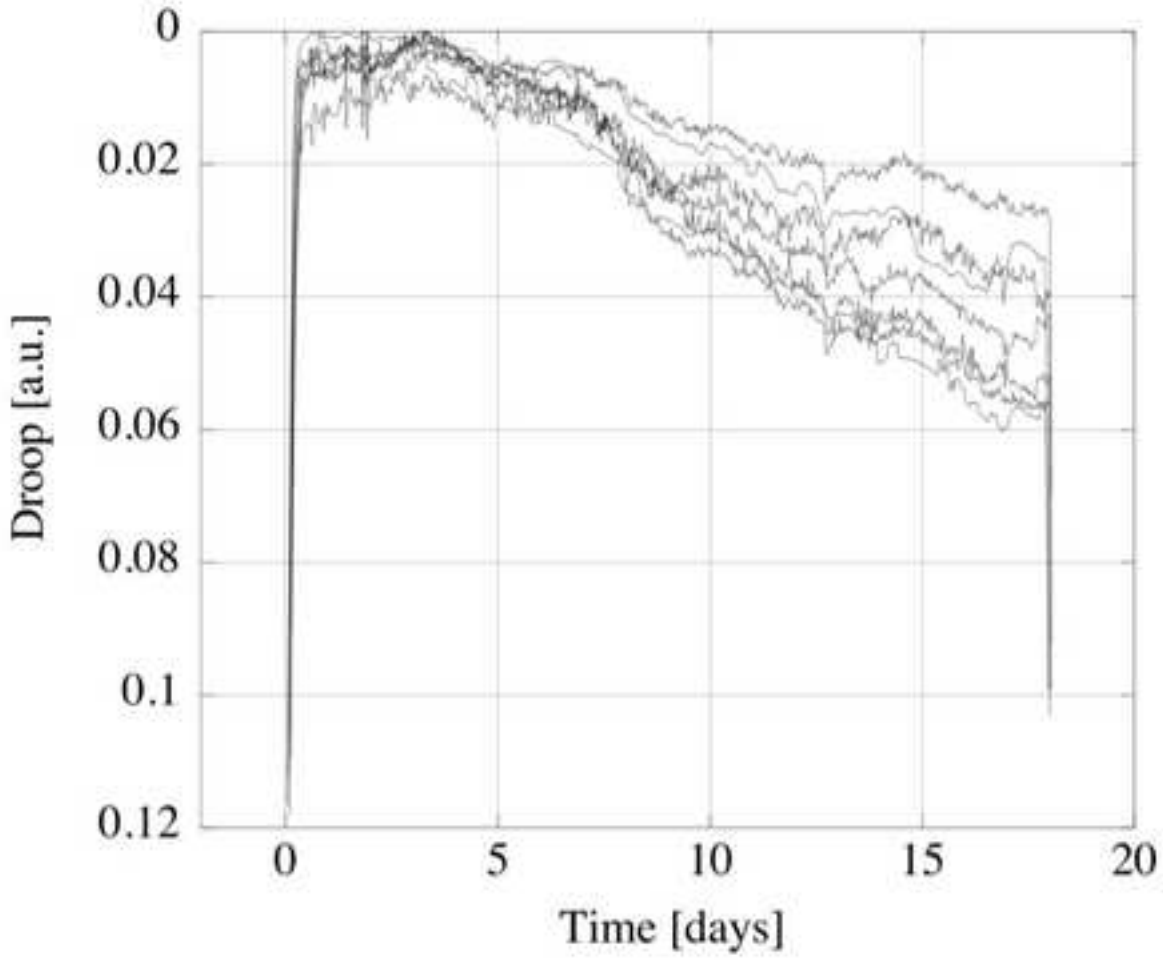

Figure 12

Click here to download high resolution image